

# Cooperative Target Capture using Voronoi Region Shaping

Gautam Kumar\* and Ashwini Ratnoo†  
*Indian Institute of Science, Bengaluru 560 012, India*

## I. Introduction

Multiplayer pursuit-evasion (MPE) scenarios have gained a lot of attention for their application in the area of missile-target interception [1], border-defence problem [2], and territory protection from aerial intruders [3]. One of its variants involves multiple pursuers and a single evader/target. Therein, the pursuers use strategies to capture an evader while the evader's job is to evade successfully or to maximize the capture time.

The earliest of the works considers a single pursuer-single evader differential game in an unbounded domain where both players employ optimal strategies to achieve their objectives [4]. A border defence differential game is considered in [5, 6] where the pursuer's task is to capture the evader infiltrating the region of interest. This problem is later explored for the MPE game in [7] where optimal strategies are devised for the pursuers to capture the evaders before they enter the restricted region. The MPE problem of capturing a single evader is formulated as a target-attacker-defender scenario in [8] where a group of pursuers lures the target to the reachable set of the remaining pursuers such that an encirclement around the target is achieved. The pursuit strategies in [4–8] require the solution of the Hamilton-Jacobi-Isaacs (HJI) equation. With multiple players in the game, the non-uniqueness of the terminal condition complicates the synthesis of strategies for the players in that approach [9]. Solving the HJI equation in an MPE game scenario is computationally expensive and realizing any cooperation among agents adds further complexity.

To overcome these limitations, various geometric approaches are presented in the literature. Ref. [10] presented a framework for capturing a target using multiple pursuers while assuming that the target is initially inside the convex hull of the pursuers. A trapping chain formation-based strategy is proposed in [11] where a bounded rectangular region is swept by a chain of UAVs leading to encirclement and capture of target. The capture of a faster evader is considered in [12] by employing a fishing strategy in which the pursuers surround the target and then shrink the encirclement region leading to the capture of the evader. That strategy requires a minimum number of pursuers and a specific initial position distribution of the pursuers around the target. Apollonius circle-based pursuit strategies for capturing a constant speed evader are investigated in [13, 14] wherein a minimum number of pursuers are required to encircle the evader at the initial time. A relay pursuit strategy for capturing a single target using multiple pursuers is proposed in [15] where a moving pursuer uses a policy that reduces the distance between the target and the stationary pursuers. The geometric approaches discussed in [11–15] consider the speed of the evader and pursuers to be constant.

---

\*Research Scholar, Department of Aerospace Engineering; gautamkumar1@iisc.ac.in.

†Associate Professor, Department of Aerospace Engineering; ratnoo@iisc.ac.in. Associate Fellow AIAA

Due to its simple construction, efficient partitioning of the region of interest, and properties that enhance cooperation among agents, the idea of Voronoi partitioning is employed in several aerospace applications such as path planning [16], airspace sectorization [17], and area coverage [18, 19]. A relay pursuit strategy is proposed in [20] wherein the region is dynamically divided using Voronoi partitioning and the pursuers are assigned targets based on the minimum capture time. Voronoi partition-based techniques are also used in MPE scenarios. A class of geometric approaches [21–25] utilize Voronoi partitioning to define the evader’s proximity region as the Voronoi cell whose generator is the evader’s position. An area minimization policy for multiple pursuers-single evader problem is presented in [21] where a guaranteed finite time capture of the evader is established, and that work is further explored for a non-convex environment in [22]. In [23, 24], a monotonic decrease in the area of the evader’s proximity region is achieved by a move-to-centroid strategy which directs a pursuer towards the center of the boundary of the Voronoi edge shared between that pursuer and the evader. For capturing an evader in an unbounded domain, the evader is first brought within the convex hull of the pursuers, and then the move-to-centroid strategy is used to deduce pursuers’ control inputs for capturing the evader [25]. In [21–25], the pursuers’ motion strategy is designed independently of the target’s motion. Further, in those works, it is assumed that the evader moves with a speed less than or equal to that of the pursuers. Consequently, the shrinkage of the evader’s proximity region is achieved by relying on the assumptions made rather than directly imposing the conditions on the system dynamics. This reflects a restrictive and indirect treatment of the problem. Additionally, the time of capture of the evader is not analyzed in the MPE strategies [21–25].

In contrast, this paper directly considers the motion of the target and vertices of its proximity region, and proposes a motion policy that guarantees a monotonic decrease in the area of the evader’s proximity region. The contributions of the work are as follows:

- 1) Given an initial position distribution of pursuers, the Voronoi Diagram is employed to characterize the evader’s proximity region. The key idea is to dynamically shape that region using a policy that directs its vertices towards its instantaneous centroid. Analysis of the resulting dynamics of the evader’s proximity region deduces the velocity control inputs for the pursuers.
- 2) Using the proposed motion policy, the evader’s proximity region is shown to shrink exponentially irrespective of its speed and evasion policy. As a result, the evader’s capture is guaranteed without prior knowledge of the bounds on the evader’s speed. Further, a conservative upper bound on the time of evader capture is deduced using the Chebyshev radius of the evader’s proximity region.
- 3) Validation studies show the capture of the evader while it moves with constant or variable speed. In one of the simulation cases, a second-order polynomial Kalman filter is employed to estimate the velocity and position of the evader using its noisy position information.

The remainder of the paper is organized as follows: Section II introduces the problem. The evader region and its dynamics are analyzed in Section III. Section IV presents the proposed motion policy which is demonstrated using

simulations in Section V. Conclusions are drawn in Section VI.

## II. Problem Statement

Consider a two-dimensional region containing  $(N + 1)$  agents with  $N(> 2)$  pursuers and 1 evader. The position of  $i$ th pursuer and the evader is denoted by  $\mathbf{x}_i^P(t) = [x_i^P, y_i^P]^T$  and  $\mathbf{x}^E(t) = [x^E, y^E]^T$ , respectively. All agents follow single integrator motion kinematics, that is,

$$\begin{aligned}\dot{\mathbf{x}}_i^P(t) &= u_i^P(t), \quad i \in \mathcal{N} = \{1, 2, \dots, N\} \\ \dot{\mathbf{x}}^E(t) &= u^E(t),\end{aligned}\tag{1}$$

where  $u_i^P, u^E \in \mathbb{R}^2$  denote  $i$ th pursuer's and the evader's velocity input, respectively. Further analysis considers the following assumptions:

- (A1) The initial position of the evader lies inside the convex hull formed by the set of pursuers' initial position.
- (A2) No two agents are initially collocated.
- (A3) The environment is obstacle-free.
- (A4) A centralized server knows agents' position and velocity information and relays the computed input to the pursuers.

The pursuers' goal is to capture the evader while it follows an evasion policy unknown to the pursuer. The evader is captured at time  $t_C \geq 0$  if the following condition satisfies:

$$\exists i : \|\mathbf{x}^E(t_C) - \mathbf{x}_i^P(t_C)\| \leq r_c, i \in \mathcal{N},\tag{2}$$

where  $r_c \in \mathbb{R}^+$  is the radius of the capture zone of pursuers. The objective here is to deduce  $u_i^P, i \in \mathcal{N}$  which leads to the capture of the evader.

## III. Evader Proximity Region

The proximity region for an agent is defined as the set of all points in  $\mathbb{R}^2$  which are closer to itself than to any other agent. Accordingly, the proximity region can be determined by *Generalised Voronoi Diagram* (GVD). The GVD partitions  $\mathbb{R}^2$  into sub-regions,  $S(\mathbf{X})$  where  $\mathbf{X}$  is the set of generators which in this case is the set of agents' position, that is,  $\mathbf{X} = \{\mathbf{x}^E, \mathbf{x}_1^P, \mathbf{x}_2^P, \dots, \mathbf{x}_N^P\}$ .

### A. Agents' Proximity Region

Given the set  $\mathbf{X}$ , the proximity region of  $i$ th agent,  $S(\mathbf{X}_i)$  is defined as

$$S(\mathbf{X}_i) = \{ \mathbf{x} : \|\mathbf{x} - \mathbf{X}_i\| \leq \|\mathbf{x} - \mathbf{X}_j\| \}, \quad i, j = \{1, 2, \dots, N+1\}, \quad i \neq j, \quad \{\mathbf{X}_i, \mathbf{X}_j\} \in \mathbf{X}. \quad (3)$$

**Property 1.** [26]  $S(\mathbf{X}_i)$  is a bounded convex region if  $\mathbf{X}_i$  lies inside the convex hull formed by the elements in  $\mathbf{X}$ .

**Property 2.** [26] Any vertex point of  $S(\mathbf{X}_i)$  is equidistant from two or more generators other than itself.

An example scenario with 4 pursuers and 1 evader, and their proximity regions generated using (3) is shown in Fig. 1. The dashed purple polygon is the convex hull formed by the agents' initial position. The yellow and blue regions represent the proximity region of the evader and the pursuers, respectively. The black solid lines represent the boundary of  $S(\mathbf{X}_i)$ ,  $\forall \mathbf{X}_i \in \mathbf{X}$ . From (A1) and Property (1),  $S(\mathbf{x}^E)$  is a bounded convex polygon.

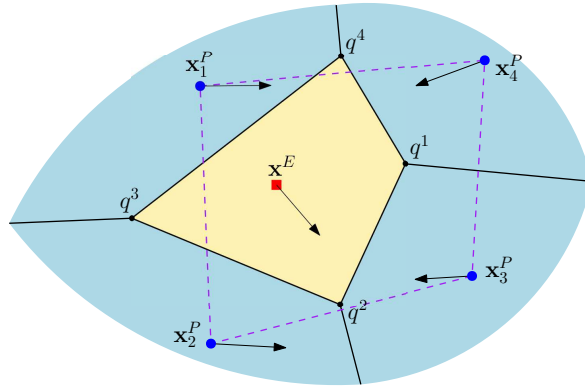


**Fig. 1** Voronoi partition with multiple agents in the region. (Square and circular markers indicate the position of the evader and pursuers, respectively.)

## B. Evader Proximity Region Dynamics

Consider the proximity region of the evader,  $S(\mathbf{x}^E)$  in Fig. 1. The set of vertices of  $S(\mathbf{x}^E)$  is denoted as  $Q = \{\mathbf{q}^1, \mathbf{q}^2, \dots, \mathbf{q}^l\}$ , where  $\mathbf{q}^i = [q_x^i, q_y^i]^T$ . The vertices are arranged in a clockwise manner about the evader's position. Using the shoelace method for calculation of the area of a polygon from its vertices, the evader area  $A_e$  is obtained as:

$$A_e = \frac{1}{2} \sum_{i=1}^l \begin{vmatrix} q_x^i & q_y^i \\ q_x^{i+1} & q_y^{i+1} \end{vmatrix}, \quad (\text{where } \mathbf{q}^{l+1} = \mathbf{q}^1) \quad (4)$$

$$= \frac{1}{2} [(q_x^1 q_y^2 + q_x^2 q_y^3 + \dots + q_x^l q_y^1) - (q_y^1 q_x^2 + q_y^2 q_x^3 + \dots + q_y^l q_x^1)] \quad (5)$$

$$= \frac{1}{2} \sum_{i=1}^l (q_x^i q_y^{i+1} - q_x^{i+1} q_y^i). \quad (6)$$

Differentiating Eq. (6), the evader area dynamics is obtained as follows:

$$\dot{A}_e = \frac{1}{2} \sum_{i=1}^l \left( \frac{\partial A_e}{\partial q_x^i} \dot{q}_x^i + \frac{\partial A_e}{\partial q_y^i} \dot{q}_y^i \right), \text{ where } \frac{\partial A_e}{\partial q_x^i} = (q_y^{i+1} - q_y^{i-1}), \quad \frac{\partial A_e}{\partial q_y^i} = (q_x^{i-1} - q_x^{i+1}), \mathbf{q}^{l+1} = \mathbf{q}^1, \mathbf{q}^0 = \mathbf{q}^l. \quad (7)$$

**Remark 1.** From Eq. (7), the rate of change of  $A_e$  depends on the position and velocity of vertices of  $S(\mathbf{x}^E)$ .

### C. Relation between Motion of Agents and Vertices of $S(\mathbf{x}^E)$

The proximity region of all pursuers in  $\mathcal{N}$  may not share boundary with  $S(\mathbf{x}^E)$ . By assumption (A1), the maximum number of such pursuers can be  $N - 3$ . Consider  $\mathcal{M}$  to be the set of  $m (\leq N)$  pursuers whose proximity region shares a common boundary with  $S(\mathbf{x}^E)$ . Accordingly, the evader area dynamics in Eq. (7) is affected only by pursuers in  $\mathcal{M}$  while the remaining pursuers are redundant and remain stationary. The pursuers in  $\mathcal{M}$  are hereinafter referred to as active pursuers.

**Remark 2.** The number of vertices of  $S(\mathbf{x}^E)$  equals the number of active pursuers, that is,  $l = m$ .

In Fig. 2,  $\mathbf{q}^{i1} = [q_x^{i1}, q_y^{i1}]^T$  and  $\mathbf{q}^{i2} = [q_x^{i2}, q_y^{i2}]^T$  denote the end points of the edge shared between  $S(\mathbf{x}_i^P)$  ( $1 \leq i \leq m$ ) and the evader. The relation between  $\{\mathbf{q}^{i1}, \mathbf{q}^{i2}\}$  and  $\mathbf{q}^j \in \mathcal{Q} (1 \leq j \leq l)$  is expressed as

$$\begin{bmatrix} \mathbf{q}^{11} \\ \mathbf{q}^{12} \\ \mathbf{q}^{21} \\ \mathbf{q}^{22} \\ \vdots \\ \mathbf{q}^{m1} \\ \mathbf{q}^{m2} \end{bmatrix} = \begin{bmatrix} \mathbf{R}^{11} \\ \mathbf{R}^{12} \\ \mathbf{R}^{21} \\ \mathbf{R}^{22} \\ \vdots \\ \mathbf{R}^{m1} \\ \mathbf{R}^{m2} \end{bmatrix} \begin{bmatrix} \mathbf{q}^1 \\ \mathbf{q}^2 \\ \vdots \\ \mathbf{q}^l \end{bmatrix}, \quad (8)$$

where  $\mathbf{R}^{ik} = [\mathbf{r}_1^{ik}, \mathbf{r}_2^{ik}, \dots, \mathbf{r}_l^{ik}]$  ( $k = \{1, 2\}$ ) is defined as

$$\mathbf{r}_j^{ik} = \begin{cases} \begin{bmatrix} 1 & 0 \\ 0 & 1 \end{bmatrix}, & \text{if } \mathbf{q}^{ik} = \mathbf{q}^j \\ \mathbf{0}_{2 \times 2}, & \text{otherwise.} \end{cases} \quad (9)$$

Consider the example shown in Fig. 2, Pursuer  $P_i$  and Evader  $E$  share the edge  $\overline{\mathbf{q}^{i1} \mathbf{q}^{i2}}$ . Using the Property 2 of

$S(\mathbf{x}^E)$ ,

$$\|\mathbf{x}_i^P - \mathbf{q}^{i1}\| = \|\mathbf{x}^E - \mathbf{q}^{i1}\|, \text{ and} \quad (10)$$

$$\|\mathbf{x}_i^P - \mathbf{q}^{i2}\| = \|\mathbf{x}^E - \mathbf{q}^{i2}\|. \quad (11)$$

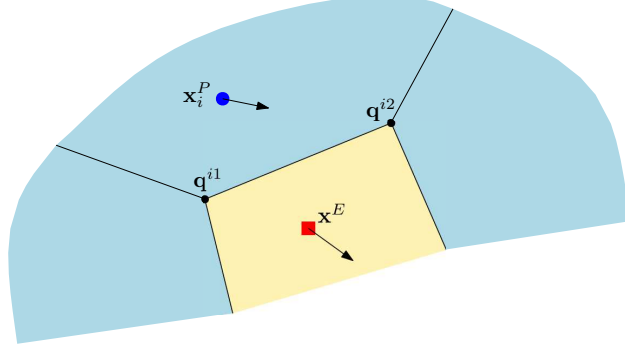


**Fig. 2** An example scenario depicting boundary shared between  $S(\mathbf{x}_i^P)$  and  $S(\mathbf{x}^E)$ .

Following relations are obtained by squaring and then differentiating both sides of Eqs. (10) and (11),

$$(\dot{x}_i^P - \dot{q}_x^{i1})(x_i^P - q_x^{i1}) + (\dot{y}_i^P - \dot{q}_y^{i1})(y_i^P - q_y^{i1}) = (\dot{x}^E - \dot{q}_x^{i1})(x^E - q_x^{i1}) + (\dot{y}^E - \dot{q}_y^{i1})(y^E - q_y^{i1}). \quad (12)$$

$$(\dot{x}_i^P - \dot{q}_x^{i2})(x_i^P - q_x^{i2}) + (\dot{y}_i^P - \dot{q}_y^{i2})(y_i^P - q_y^{i2}) = (\dot{x}^E - \dot{q}_x^{i2})(x^E - q_x^{i2}) + (\dot{y}^E - \dot{q}_y^{i2})(y^E - q_y^{i2}). \quad (13)$$

Rearranging terms in Eqs. (12) and (13), the velocity input to  $P_i$ ,  $u_i^P = [\dot{x}_i^P, \dot{y}_i^P]^T$  can be deduced in terms of position and velocity of the evader and vertices of  $S(\mathbf{x}^E)$  as follows:

$$u_i^P = A_i^{-1} B_i \begin{bmatrix} \dot{\mathbf{q}}^{i1} \\ \dot{\mathbf{q}}^{i2} \end{bmatrix} + A_i^{-1} C_i \dot{\mathbf{x}}^E, \quad (14)$$

where matrices  $A_i \in \mathbb{R}^{2 \times 2}$ ,  $B_i \in \mathbb{R}^{2 \times 4}$ , and  $C_i \in \mathbb{R}^{2 \times 2}$  are as follows:

$$A_i = \begin{bmatrix} x_i^P - q_x^{i1} & y_i^P - q_y^{i1} \\ x_i^P - q_x^{i2} & y_i^P - q_y^{i2} \end{bmatrix}, \quad B_i = \begin{bmatrix} x_i^P - x^E & y_i^P - y^E & 0 & 0 \\ 0 & 0 & x_i^P - x^E & y_i^P - y^E \end{bmatrix}, \quad C_i = \begin{bmatrix} x^E - q_x^{i1} & y^E - q_y^{i1} \\ x^E - q_x^{i2} & y^E - q_y^{i2} \end{bmatrix}. \quad (15)$$

Differentiating Eq. (8) and using that in Eq. (14) leads to

$$u_i^P = A_i^{-1} B_i \begin{bmatrix} \mathbf{R}^{i1} \\ \mathbf{R}^{i2} \\ \vdots \\ \mathbf{R}^{il} \end{bmatrix} \begin{bmatrix} \dot{\mathbf{q}}^1 \\ \dot{\mathbf{q}}^2 \\ \vdots \\ \dot{\mathbf{q}}^l \end{bmatrix} + A_i^{-1} C_i \dot{\mathbf{x}}^E. \quad (16)$$

Using Eq. (16), the velocity input for active pursuers can be expressed as

$$\begin{bmatrix} u_1^P \\ u_2^P \\ \vdots \\ u_m^P \end{bmatrix} = \begin{bmatrix} A_1^{-1} B_1 & \mathbf{0}_{2 \times 4} & \dots & \mathbf{0}_{2 \times 4} \\ \mathbf{0}_{2 \times 4} & A_2^{-1} B_2 & \dots & \mathbf{0}_{2 \times 4} \\ \vdots & \vdots & \ddots & \vdots \\ \mathbf{0}_{2 \times 4} & \mathbf{0}_{2 \times 4} & \dots & A_m^{-1} B_m \end{bmatrix} \begin{bmatrix} \mathbf{R}^{11} \\ \mathbf{R}^{12} \\ \mathbf{R}^{21} \\ \mathbf{R}^{22} \\ \vdots \\ \mathbf{R}^{m1} \\ \mathbf{R}^{m2} \end{bmatrix} \begin{bmatrix} \dot{\mathbf{q}}^1 \\ \dot{\mathbf{q}}^2 \\ \vdots \\ \dot{\mathbf{q}}^l \end{bmatrix} + \begin{bmatrix} A_1^{-1} C_1 & \mathbf{0}_{2 \times 2} & \dots & \mathbf{0}_{2 \times 2} \\ \mathbf{0}_{2 \times 2} & A_2^{-1} C_2 & \dots & \mathbf{0}_{2 \times 2} \\ \vdots & \vdots & \ddots & \vdots \\ \mathbf{0}_{2 \times 2} & \mathbf{0}_{2 \times 2} & \dots & A_m^{-1} C_m \end{bmatrix} \begin{bmatrix} \dot{\mathbf{x}}^E \\ \dot{\mathbf{x}}^E \\ \vdots \\ \dot{\mathbf{x}}^E \end{bmatrix}. \quad (17)$$

#### IV. Proposed Motion Policy

Based on a geometric motion policy for the vertices of  $S(\mathbf{x}^E)$ , this section presents a control law for the pursuers. Consider  $\mathbf{x}_C = [x_C, y_C]$  denotes the centroid of  $S(\mathbf{x}^E)$ . The desired motion policy directs  $i$ th vertex of  $S(\mathbf{x}^E)$  towards  $\mathbf{x}_C$  and is expressed as follows:

$$\dot{\mathbf{q}}^i = \begin{bmatrix} \dot{q}_x^i \\ \dot{q}_y^i \end{bmatrix} = K \begin{bmatrix} x_C - q_x^i \\ y_C - q_y^i \end{bmatrix}, \quad \forall i = 1, 2, \dots, l, \quad (18)$$

where  $K$  is a positive scalar. A geometric representation of the vertex motion policy is shown in Fig. 3.

**Theorem 1.** *For the motion policy proposed in Eq. (18), the evader area,  $A_e$  decreases monotonically with time.*

*Proof.* Substituting for  $\dot{\mathbf{q}}_i$  from Eq. (18) in Eq. (7), the evader area dynamics can be expressed as

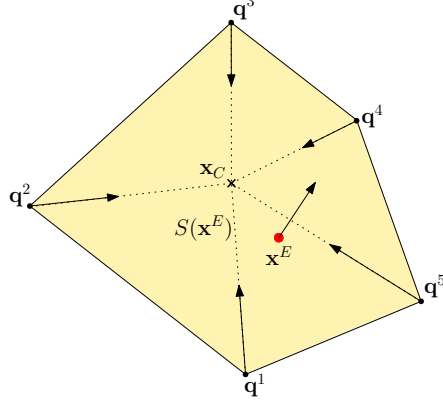


Fig. 3 Motion policy for the vertices of  $S(x^E)$ .

$$\dot{A}_e = \frac{1}{2} \sum_{i=1}^l \left( -K \frac{\partial A_e}{\partial q_x^i} (q_x^i - x_C) - K \frac{\partial A_e}{\partial q_y^i} (q_y^i - y_C) \right) \quad (19)$$

$$= \frac{-K}{2} \sum_{i=1}^l \left( (q_x^i - x_C)(q_y^{i+1} - q_y^{i-1}) + (q_y^i - y_C)(q_x^{i-1} - q_x^{i+1}) \right) \quad (20)$$

$$= \frac{-K}{2} \sum_{i=1}^l (q_x^i (q_y^{i+1} - q_y^{i-1}) + q_y^i (q_x^{i-1} - q_x^{i+1})) + \frac{K}{2} \sum_{i=1}^l (x_C (q_y^{i+1} - q_y^{i-1}) + y_C (q_x^{i-1} - q_x^{i+1})). \quad (21)$$

Since  $\sum_{i=1}^l x_C (q_y^{i+1} - q_y^{i-1}) = \sum_{i=1}^l y_C (q_x^{i-1} - q_x^{i+1}) = 0$ , Eq. (21) reduces to

$$\dot{A}_e = \frac{-K}{2} \sum_{i=1}^l \left( q_x^i (q_y^{i+1} - q_y^{i-1}) + q_y^i (q_x^{i-1} - q_x^{i+1}) \right). \quad (22)$$

Rearranging Eq. (5), the evader area can be expressed as

$$A_e = \frac{1}{4} [2(q_x^1 q_y^2 + q_x^2 q_y^3 + \dots + q_x^l q_y^1) - 2(q_y^1 q_x^2 + q_y^2 q_x^3 + \dots + q_y^l q_x^1)] \quad (23)$$

$$= \frac{1}{4} [q_x^1 (q_y^2 - q_y^l) + q_x^2 (q_y^3 - q_y^1) + \dots + q_x^l (q_y^1 - q_y^{l-1}) + q_y^1 (q_x^l - q_x^2) + q_y^2 (q_x^1 - q_x^3) + \dots + q_y^l (q_x^{l-1} - q_x^1)] \quad (24)$$

$$= \frac{1}{4} \sum_{i=1}^l \left( q_x^i (q_y^{i+1} - q_y^{i-1}) + q_y^i (q_x^{i-1} - q_x^{i+1}) \right). \quad (25)$$

Using Eqs. (22) and (25), the evader area dynamics is governed by

$$\begin{aligned} \dot{A}_e &= -2KA_e \\ \implies A_e(t) &= A_e(0) \exp(-2Kt), \end{aligned} \quad (26)$$

where  $A_e(0)$  is the area of  $S(\mathbf{x}^E)$  at  $t = 0$ . □

**Remark 3.** Using Eq. (26), it can be noted that the evader area decreases exponentially with time irrespective of the evader's evasion policy and speed.

The pursuers' velocity input is obtained by substituting for  $\mathbf{q}_i$  from Eq. (18) into Eq. (17) as

$$u_i^P = \begin{cases} \text{RHS of Eq. (17) where } \mathbf{q}_i \text{ satisfies Eq. (18),} & \text{if } \mathbf{x}_i^P \in \mathcal{M} \\ [0, 0]^T, & \text{otherwise} \end{cases} \quad (27)$$

**Proposition 1.** For the proposed control law in Eq. (27), the capture of the evader is guaranteed.

*Proof.* Let  $R_{\min}$  denote the separation between the evader and its closest pursuer. By virtue of Voronoi partitioning, the pursuer's position is the mirror image of the evader's position about the edge shared between them. Accordingly,

$$R_{\min} = 2 \min \| \mathbf{x}^E - \mathcal{V}(\mathbf{x}^E) \|, \quad (28)$$

where  $\mathcal{V}(\mathbf{x}^E) = \{ \mathbf{x} : \| \mathbf{x} - \mathbf{x}^E \| = \| \mathbf{x} - \mathbf{x}_i^P \|, \forall \mathbf{x}_i^P \in \mathcal{M} \}$ . Using Eq. (26), since  $A_e \rightarrow 0$ , the distance of the evader from the boundary of  $S(\mathbf{x}^E)$ , that is,  $\min \| \mathbf{x}^E - \mathcal{V}(\mathbf{x}^E) \| \rightarrow 0$  and hence  $R_{\min} \rightarrow 0$ . □

While Proposition 1 presents a guarantee for target capture as  $t \rightarrow \infty$ , an upper bound on the capture time is deduced subsequently.

**Definition 1.** For a convex polygon  $\mathcal{P}$ , the Chebyshev center is the center of the optimal circle or the largest circle drawn within  $\mathcal{P}$  and the Chebyshev radius is the radius of that circle.

**Property 3.** [27] The Chebyshev center  $\mathbf{x}_{cb}$  is also the point farthest from the boundary of  $\mathcal{P}$ .

**Property 4.** [28] In the family of all  $m$ -sided convex polygons containing a given circle, the regular polygon that circumscribes the circle has the least area.

**Lemma 1.** Consider two  $m$ -sided convex polygons ( $m > 2$ ),  $\mathcal{P}_1$  and  $\mathcal{P}_2$  with equal areas where  $\mathcal{P}_1$  is regular and  $\mathcal{P}_2$  is irregular. The Chebyshev radius of  $\mathcal{P}_1$  is greater than that of  $\mathcal{P}_2$ .

*Proof.* Let the Chebyshev radius of  $\mathcal{P}_1$  and  $\mathcal{P}_2$  be  $r_1$  and  $r_2$ , respectively. Using Property 4, there exists an  $m$ -sided regular polygon  $\mathcal{P}_3$  which circumscribes a circle of radius  $r_2$  but has a lesser area than  $\mathcal{P}_2$  as illustrated in Fig. 4. Consider  $A_{\mathcal{P}_1}$ ,  $A_{\mathcal{P}_2}$  and  $A_{\mathcal{P}_3}$  are the areas of the polygons  $\mathcal{P}_1$ ,  $\mathcal{P}_2$  and  $\mathcal{P}_3$ , respectively. Using the relation between the area of a regular polygon and the radius of its inscribed circle [29], the radii  $r_1$  and  $r_2$  are given by

$$r_1 = \sqrt{\frac{A_{\mathcal{P}_1}}{m \tan\left(\frac{\pi}{m}\right)}}, \quad r_2 = \sqrt{\frac{A_{\mathcal{P}_3}}{m \tan\left(\frac{\pi}{m}\right)}}. \quad (29)$$

Since  $A_{\mathcal{P}_1} = A_{\mathcal{P}_2} > A_{\mathcal{P}_3}$ , using Eq. (29), the Chebyshev radius of  $\mathcal{P}_1$  is greater than that of  $\mathcal{P}_2$ , that is,  $r_1 > r_2$ .

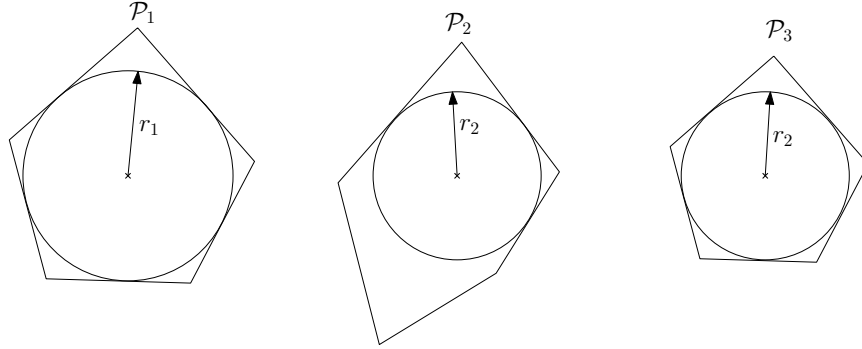


**Fig. 4** Comparison of the Chebyshev radii of  $\mathcal{P}_1, \mathcal{P}_2, \mathcal{P}_3$  ( $A_{\mathcal{P}_1} = A_{\mathcal{P}_2} > A_{\mathcal{P}_3}$ ).

□

Using Lemma 1, for a specific value of  $A_e$ , the Chebyshev radius is maximum when  $S(\mathbf{x}^E)$  is a regular polygon. Further, the distance between the evader and a pursuer is twice that between the evader and the corresponding shared side of  $S(\mathbf{x}_E)$ . To find the upper bound on the capture time, subsequent analysis considers the following assumptions:

(A5) The evader always lies at the Chebyshev center of  $S(\mathbf{x}_E)$ .

(A6)  $S(\mathbf{x}_E)$  is considered as an  $m$ -sided regular polygon at all times.

Fig. 5 depicts the largest possible circle drawn in  $S(\mathbf{x}^E)$  of area  $A_e$  with  $R_M$  being the Chebyshev radius of  $S(\mathbf{x}^E)$ .

Using Eq. (28) and Property 3,

$$R_{\min} = 2R_M. \quad (30)$$

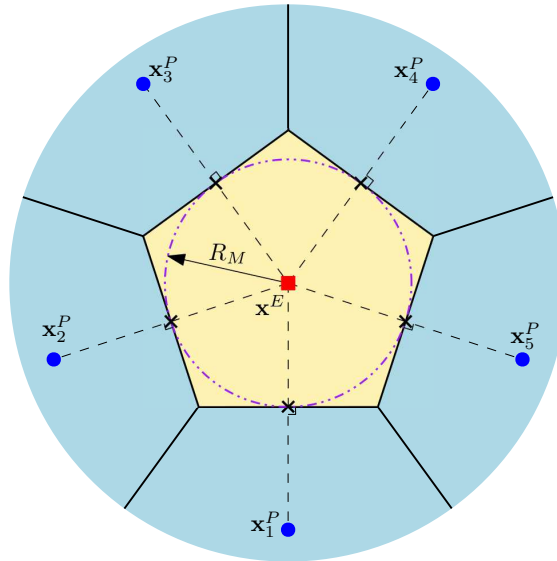


**Fig. 5** Largest possible circle drawn in  $S(\mathbf{x}_E)$  considering  $\mathbf{x}_E$  as the Chebyshev center.

**Proposition 2.** For the proposed policy, the upper bound on the time of evader capture is

$$t_C^U = -\frac{1}{2K} \log \left( \frac{mr_c^2}{4A_e(0)} \tan \left( \frac{\pi}{m} \right) \right). \quad (31)$$

*Proof.* Using the assumptions (A5), (A6) and Eq. (29), the Chebyshev radius is expressed in terms of  $A_e(t)$  as follows:

$$R_M(t) = \sqrt{\frac{A_e(t)}{m \tan \left( \frac{\pi}{m} \right)}}. \quad (32)$$

Using Eqs. (26) and (32),

$$R_M(t) = \sqrt{\frac{A_e(0) \exp(-2Kt)}{m \tan \left( \frac{\pi}{m} \right)}}. \quad (33)$$

Using Eqs. (2) and (30), the capture criteria can be expressed in terms of  $R_M$  as

$$r_c = 2R_M. \quad (34)$$

Using Eqs. (33) and (34),

$$\sqrt{\frac{A_e(0) \exp(-2Kt_C^U)}{m \tan \left( \frac{\pi}{m} \right)}} = \frac{r_c}{2}, \quad (35)$$

$$\Rightarrow t_C^U = -\frac{1}{2K} \log \left( \frac{mr_c^2}{4A_e(0)} \tan \left( \frac{\pi}{m} \right) \right). \quad (36)$$

□

## V. Simulation Results

To demonstrate the characteristics of the proposed motion policy, this section presents simulation results considering 3 pursuers. The capture radius  $r_c = 0.2$  m. The constant gain used in (18) satisfies  $K = 0.05$ . In all simulations, the pursuers' initial positions are (-80.65 m, 44.48 m), (63.63 m, -70.02 m) and (63.51 m, 31.92 m), and the evader's initial position is (0.7438 m, 18.92 m). For the resulting Voronoi partition at  $t = 0$ ,  $A_e(0) = 13370$  m<sup>2</sup> and  $m = 3$ . Accordingly, the upper bound on the time of evader capture calculated using Eq. (31) is 124.58 s.

### A. Case 1: Non-maneuvering Evader

Here, the evader follows a straight line path with constant velocity,  $u^E = [-1.8, -2.5]$  m/s. The trajectory plot for the agents is shown in Fig. 6. The colour of solid lines depicting agents' trajectory darkens with time which shows the spatio-temporal information of their position. Square and asterisk markers depict the start and end position of the

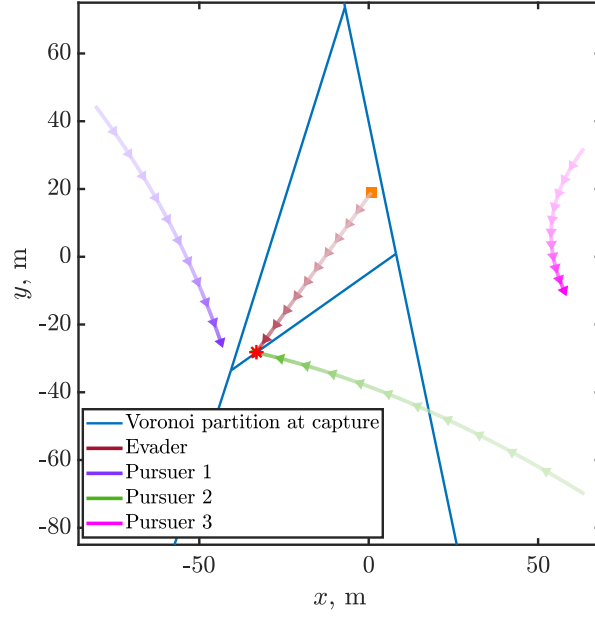


**Fig. 6 Case 1: Agents' trajectory .**

evader, respectively. As shown in Fig. 7a, the evader area exponentially decreases with time. The separation between the evader and the closest pursuer in Fig. 7b shows that the evader is captured at  $t = 18.823$  s. The speed profile of the pursuers is shown in Fig. 8. In this case, it can be observed that Pursuer 1 and Pursuer 2 move at speeds faster than that of the evader. However, the speed of Pursuer 3 remains lower than that of the evader for  $t \in [0.6, 18.823]$  s.

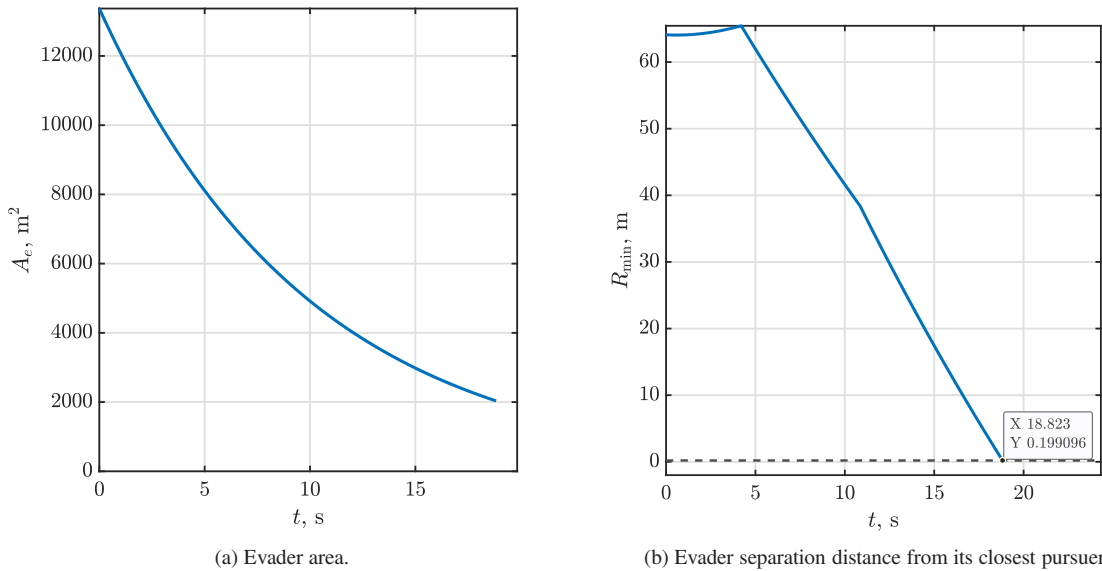


**Fig. 7 Case 1: Evader capture parameters.**

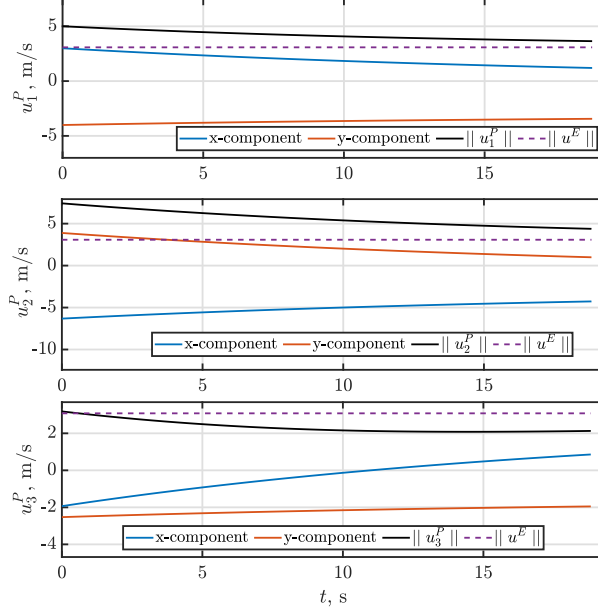


**Fig. 8 Case 1: Pursuers' velocity profile.**

### B. Case 2: Maneuvering Evader

In this case, the velocity profile of the evader is considered as  $u^E = [-2.5 \sin(0.06t), -2.5 \cos(0.06t)]^T$  m/s. The trajectory plot for the agents in Fig. 9 shows that the evader is captured by Pursuer 1. The area of the evader's proximity region is shown to shrink exponentially with time in Fig. 10a. The distance between the evader and its closest pursuer in Fig. 10b shows that the capture happens at  $t = 23.546$  s. Further, two specific evasion policies are considered, and the capture time is analyzed for each of these policies.

Policy (1) Evader moves to the centroid of  $S(\mathbf{x}^E)$  [23]: The evader's control input is given as  $u^E = 0.2(\mathbf{x}_C - \mathbf{x}^E)$ .

The resulting capture time of the evader  $t_C = 114.67$  s.

Policy (2) Evader moves to the Chebyshev center of  $S(\mathbf{x}^E)$ : Here,  $u^E = 0.2(\mathbf{x}_{cb} - \mathbf{x}^E)$  and  $t_C = 118.3$  s.

It can be seen that the use of Policy (1) or Policy (2) increases the capture time. However, the capture time is lower than the upper bound  $t_C^U = 124.58$  s as obtained through the analytic result in Eq. (31).

### C. Case 3: Maneuvering Target Capture using Noisy Position Information

As per Eq. (17), the pursuers' velocity input is computed while assuming that the evader's position and velocity information is known. In this case study, we consider a realistic scenario where the evader's position is the only information available. Kalman filtering techniques are widely used in the estimation of unknown system states of a target from noisy measurement data [30–32]. To demonstrate the effectiveness of the proposed strategy in such a scenario, a discrete second-order polynomial Kalman filter [32] is used hereinafter to estimate the evader's position and velocity information from its noisy position information.

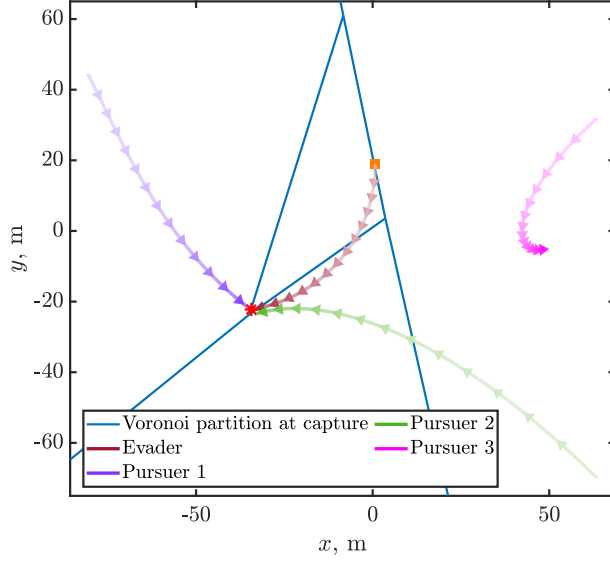


**Fig. 9 Case 2: Agents' trajectory.**

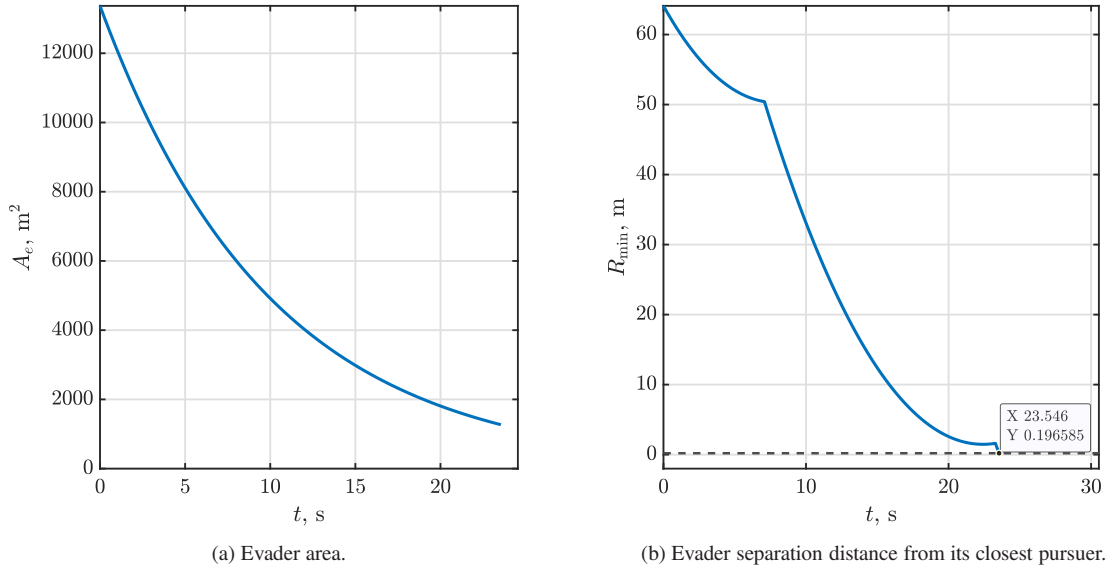


**Fig. 10 Case 2: Evader capture parameters.**

### 1. Second-order Polynomial Kalman Filter

Consider the evader state  $\mathbf{x}_k^E = [x_k^E, \dot{x}_k^E, \ddot{x}_k^E, y_k^E, \dot{y}_k^E, \ddot{y}_k^E]$  at time step  $k$ . In the case of no deterministic disturbance and control input, the discrete Kalman-filtering equation is given by

$$\hat{\mathbf{x}}_k^E = \Phi_k \hat{\mathbf{x}}_{k-1}^E + \mathbf{K}_k (\mathbf{z}_k - \mathbf{H} \Phi_k \hat{\mathbf{x}}_{k-1}^E), \quad (37)$$

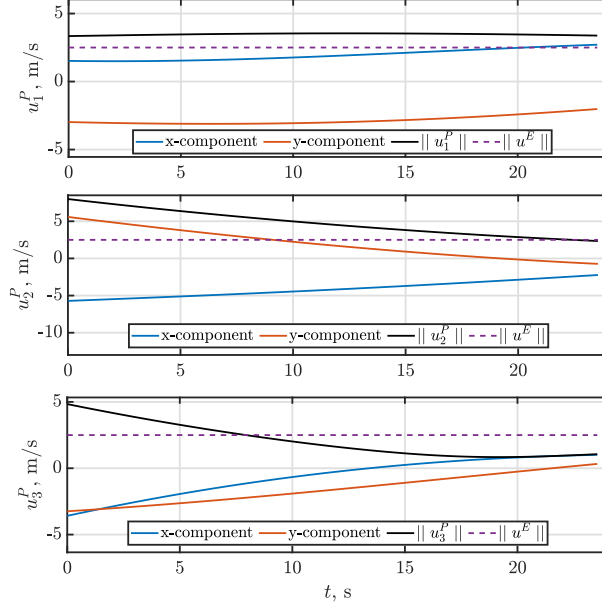


**Fig. 11 Case 2: Pursuers' velocity profile.**

where  $\hat{\mathbf{x}}_k^E$  is the estimated evader state,  $\Phi_k$  is the state transition matrix,  $\mathbf{K}_k$  is the Kalman gain matrix,  $\mathbf{z}_k$  is the measurement vector containing noisy position information and  $\mathbf{H}$  is the measurement matrix. Here,

$$\Phi_k = \begin{bmatrix} 1 & \Delta t & 0.5\Delta t^2 & 0 & 0 & 0 \\ 0 & 1 & \Delta t & 0 & 0 & 0 \\ 0 & 0 & 1 & 0 & 0 & 0 \\ 0 & 0 & 0 & 1 & \Delta t & 0.5\Delta t^2 \\ 0 & 0 & 0 & 0 & 1 & \Delta t \\ 0 & 0 & 0 & 0 & 0 & 1 \end{bmatrix}, \mathbf{H} = \begin{bmatrix} 1 & 0 & 0 & 0 & 0 & 0 \\ 0 & 0 & 0 & 1 & 0 & 0 \end{bmatrix}, \quad (38)$$

where  $\Delta t$  is the time step size. The Kalman gain matrix is computed using a set of recursive matrix equations called Riccati equations given by

$$\mathbf{M}_k = \Phi_k \mathbf{P}_{k-1} \Phi_k^T + \mathbf{Q}_k \quad (39)$$

$$\mathbf{K}_k = \mathbf{M}_k \mathbf{H}^T \left( \mathbf{H} \mathbf{M}_k \mathbf{H}^T + \mathbf{R}_k \right)^{-1} \quad (40)$$

$$\mathbf{P}_k = (\mathbf{I} - \mathbf{K}_k \mathbf{H}) \mathbf{M}_k, \quad (41)$$

where  $\mathbf{P}_k$  is the error covariance matrix after an update,  $\mathbf{M}_k$  is the error covariance matrix before an update,  $\mathbf{R}_k$  is the measurement noise matrix, and  $\mathbf{Q}_k$  is the process noise matrix. The estimated evader position and velocity information, that is,  $[\hat{x}_k^E, \hat{\dot{x}}_k^E, \hat{y}_k^E, \hat{\dot{y}}_k^E]$  as obtained from Eq. (37) is used in Eq. (17) to determine pursuers' velocity inputs.

## 2. Simulation Scenario

In this example, the evader follows a sinusoidal path governed by  $u^E = [3.89 \sin(0.7t) - 2.12, -3.89 \sin(0.7t) - 2.12]^T$  m/s. To incorporate white Gaussian noise in the position information of the evader, *awgn* function is utilized with the signal-to-noise ratio of 20 dB in MATLAB<sup>®</sup>. The trajectory plot in Fig. 12 shows that the evader is captured by Pursuer 1. The variation of the area of the evader's proximity region with time is shown in Fig. 13a. The time evolution of the separation between the evader and its closest pursuer in Fig. 13b shows that the time of evader capture is 17.654 s. The velocity profile for all pursuers is shown in Fig. 14.

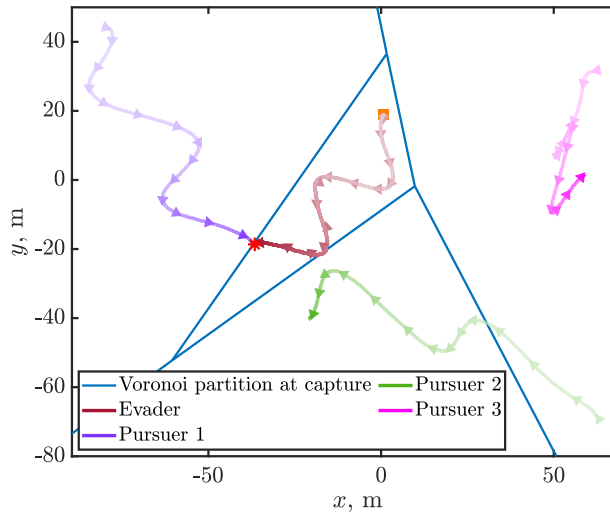


**Fig. 12 Case 3: Agents' trajectory.**

## VI. Conclusion

This paper addresses the multiple pursuers-single evader problem in an unbounded region where it is assumed that the evader's initial position lies inside the convex hull formed by the pursuers' initial position. The evader's proximity region is defined using the Voronoi partition of the plane containing the agents. A direct relationship between the velocity and position of active pursuers, evader, and vertices of the evader's proximity region is derived. The proposed motion policy directs the vertices of the evader's proximity region towards its centroid, and the corresponding velocity inputs for the active pursuers is deduced. The proposed approach guarantees an exponential reduction in the area of the evader's proximity region regardless of its motion policy. An upper bound on the time of evader capture is deduced using the limiting geometry of the evader's proximity region and its Chebyshev radius. Simulation results

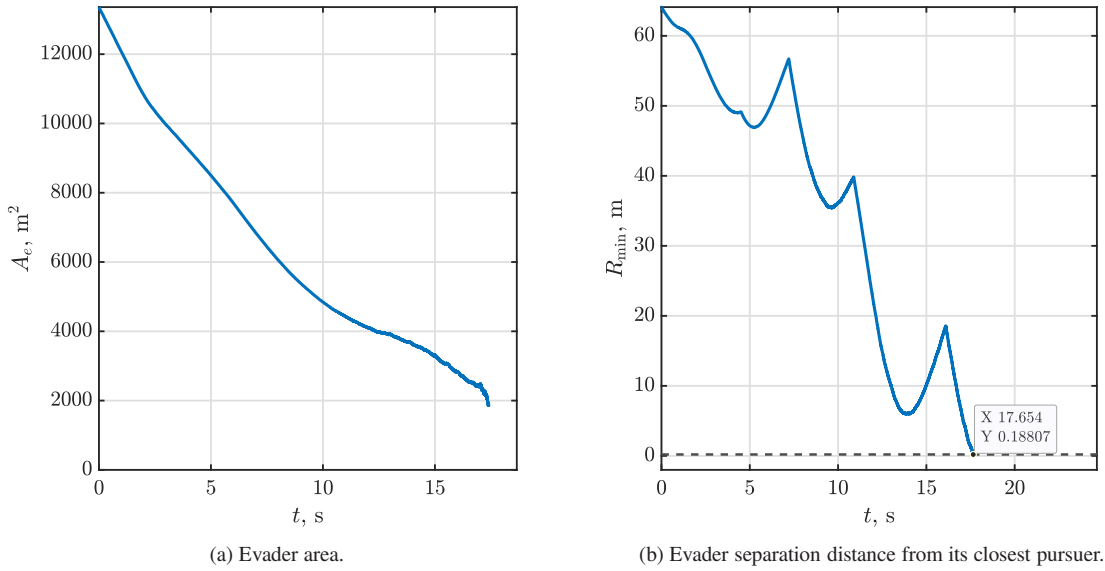


**Fig. 13 Case 3: Evader capture parameters.**

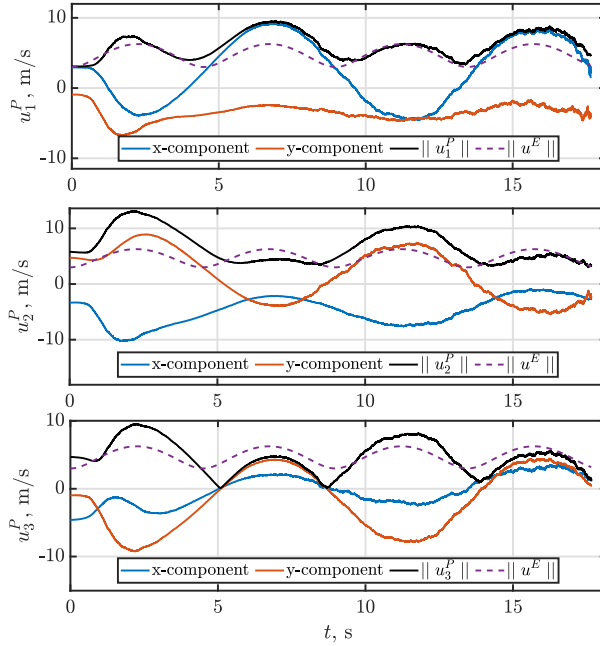


**Fig. 14 Case 3: Pursuers' velocity profile.**

illustrate that, following the proposed approach, it is not necessary for all pursuers to move faster than the evader. Further, a second-order polynomial Kalman filter is utilized in the scenario where only noisy position information of the evader is available. Future research direction can be towards exploring this strategy for capturing multiple evaders in a three-dimensional environment.

## References

- [1] Dong, W., Wang, C., Wang, J., and Xin, M., “Three-Dimensional Nonsingular Cooperative Guidance Law with Different Field-of-View Constraints,” *Journal of Guidance, Control, and Dynamics*, Vol. 44, No. 11, Nov. 2021, pp. 2001–2015. <https://doi.org/10.2514/1.G005971>.
- [2] Von Moll, A., Garcia, E., Casbeer, D., Suresh, M., and Swar, S. C., “Multiple-Pursuer, Single-Evader Border Defense Differential Game,” *Journal of Aerospace Information Systems*, Vol. 17, No. 8, Aug. 2020, pp. 407–416. <https://doi.org/10.2514/1.I010740>.
- [3] Chakravarthy, A., and Ghose, D., “Collision Cone-Based Net Capture of a Swarm of Unmanned Aerial Vehicles,” *Journal of Guidance, Control, and Dynamics*, Vol. 43, No. 9, Sep. 2020, pp. 1688–1710. <https://doi.org/10.2514/1.G004626>.
- [4] Isaacs, R., *Differential Games: A Mathematical Theory with Applications to Warfare and Pursuit, Control and Optimization*, John Wiley and Sons, 1967. <https://doi.org/10.1088/0031-9112/17/2/009>, [retrieved 3 Jun. 2024].
- [5] Garcia, E., Casbeer, D. W., and Pachter, M., “Optimal Strategies of the Differential Game in a Circular Region,” *IEEE Control Systems Letters*, Vol. 4, No. 2, Dec. 2019, pp. 492–497. <https://doi.org/10.1109/LCSYS.2019.2963173>.
- [6] Yan, R., Shi, Z., and Zhong, Y., “Defense Game in a Circular Region,” *Proceedings IEEE 56th Annual Conference on Decision and Control (CDC)*, Inst. of Electrical and Electronics Engineers, New York, Dec. 2017, pp. 5590–5595. <https://doi.org/10.1109/CDC.2017.8264502>.
- [7] Garcia, E., Casbeer, D. W., Von Moll, A., and Pachter, M., “Multiple Pursuer Multiple Evader Differential Games,” *IEEE Transactions on Automatic Control*, Vol. 66, No. 5, Jun. 2020, pp. 2345–2350. <https://doi.org/10.1109/TAC.2020.3003840>.
- [8] Wei, X., and Yang, J., “Optimal Strategies for Multiple Unmanned Aerial Vehicles in a Pursuit/Evasion Differential Game,” *Journal of Guidance, Control, and Dynamics*, Vol. 41, No. 8, Aug. 2018, pp. 1799–1806. <https://doi.org/10.2514/1.G003480>.
- [9] Yan, R., Shi, Z., and Zhong, Y., “Task Assignment for Multiplayer Reach–Avoid Games in Convex Domains via Analytical Barriers,” *IEEE Transactions on Robotics*, Vol. 36, No. 1, Sep. 2019, pp. 107–124. <https://doi.org/10.1109/TRO.2019.2935345>.
- [10] Kopparty, S., and Ravishankar, C. V., “A Framework for Pursuit Evasion Games in  $R^n$ ,” *Information Processing Letters*, Vol. 96, No. 3, Nov. 2005, pp. 114–122. <https://doi.org/10.1016/j.ipl.2005.04.012>.
- [11] Bopardikar, S. D., Bullo, F., and Hespanha, J. P., “On Discrete-Time Pursuit-Evasion Games with Sensing Limitations,” *IEEE Transactions on Robotics*, Vol. 24, No. 6, Oct. 2008, pp. 1429–1439. <https://doi.org/10.1109/TRO.2008.2006721>.
- [12] Chen, J., Zha, W., Peng, Z., and Gu, D., “Multi-Player Pursuit–Evasion Games with One Superior Evader,” *Automatica*, Vol. 71, Sep. 2016, pp. 24–32. <https://doi.org/10.1016/j.automatica.2016.04.012>.
- [13] Ramana, M., and Kothari, M., “Pursuit Strategy to Capture High-speed Evaders Using Multiple Pursuers,” *Journal of Guidance, Control, and Dynamics*, Vol. 40, No. 1, Jan. 2017, pp. 139–149. <https://doi.org/10.2514/1.G000584>.

- [14] Sun, Z., Sun, H., Li, P., and Zou, J., “Cooperative Strategy for Pursuit-Evasion Problem with Collision Avoidance,” *Ocean Engineering*, Vol. 266, Dec. 2022, p. 112742. <https://doi.org/10.1016/j.oceaneng.2022.112742>.
- [15] Pan, T., and Yuan, Y., “A Region-Based Relay Pursuit Scheme for a Pursuit–Evasion Game with a Single Evader and Multiple Pursuers,” *IEEE Transactions on Systems, Man, and Cybernetics: Systems*, Vol. 53, No. 3, Oct. 2022, pp. 1958–1969. <https://doi.org/10.1109/TSMC.2022.3210022>.
- [16] Upadhyay, S., and Aguiar, A. P., “A Voronoi-Based Safe Waypoint Generator for Hopping Robots Exploring Large Celestial Bodies,” *AIAA Scitech 2021 Forum*, Jan. 2021, p. 2015. <https://doi.org/10.2514/6.2021-2015>.
- [17] Xue, M., “Airspace Sector Redesign Based on Voronoi Diagrams,” *Journal of Aerospace Computing, Information, and Communication*, Vol. 6, No. 12, Dec. 2009, pp. 624–634. <https://doi.org/10.2514/1.41159>.
- [18] Lum, C. W., Vagners, J., and Rysdyk, R. T., “Search Algorithm for Teams of Heterogeneous Agents with Coverage Guarantees,” *Journal of Aerospace Computing, Information, and Communication*, Vol. 7, No. 1, Jan. 2010, pp. 1–31. <https://doi.org/10.2514/1.44088>.
- [19] Dong, L., Chai, S., Zhang, B., Nguang, S. K., and Li, X., “Cooperative Relay Tracking Strategy for Multi-Agent Systems with Assistance of Voronoi Diagrams,” *Journal of the Franklin Institute*, Vol. 353, No. 17, Nov. 2016, pp. 4422–4441. <https://doi.org/10.1016/j.jfranklin.2016.07.023>.
- [20] Bakolas, E., and Tsiotras, P., “Relay Pursuit of a Maneuvering Target using Dynamic Voronoi Diagrams,” *Automatica*, Vol. 48, No. 9, Sep. 2012, pp. 2213–2220. <https://doi.org/10.1016/j.automatica.2012.06.003>.
- [21] Huang, H., Zhang, W., Ding, J., Stipanović, D. M., and Tomlin, C. J., “Guaranteed Decentralized Pursuit-Evasion in the Plane with Multiple Pursuers,” *Proceedings 2011 50th IEEE Conference on Decision and Control and European Control Conference*, Inst. of Electrical and Electronics Engineers, New York, Dec. 2011, pp. 4835–4840. <https://doi.org/10.1109/CDC.2011.6161237>.
- [22] Zhou, Z., Zhang, W., Ding, J., Huang, H., Stipanović, D. M., and Tomlin, C. J., “Cooperative Pursuit with Voronoi Partitions,” *Automatica*, Vol. 72, Oct. 2016, pp. 64–72. <https://doi.org/10.1016/j.automatica.2016.05.007>.
- [23] Pierson, A., Wang, Z., and Schwager, M., “Intercepting Rogue Robots: An Algorithm for Capturing Multiple Evaders with Multiple Pursuers,” *IEEE Robotics and Automation Letters*, Vol. 2, No. 2, Dec. 2016, pp. 530–537. <https://doi.org/10.1109/LRA.2016.2645516>.
- [24] Shah, K., and Schwager, M., “Grape: Geometric Risk-Aware Pursuit-Evasion,” *Robotics and Autonomous Systems*, Vol. 121, Nov. 2019, p. 103246. <https://doi.org/10.1016/j.robot.2019.07.016>.
- [25] Wang, X., Xi, L., Ding, Y., and Chen, B. M., “Distributed Encirclement and Capture of Multiple Pursuers With Collision Avoidance,” *IEEE Transactions on Industrial Electronics*, Aug. 2023. <https://doi.org/10.1109/TIE.2023.3301511>.

- [26] Preparata, F. P., and Shamos, M. I., *Computational Geometry: an Introduction*, Springer Science & Business Media, 2012. <https://doi.org/10.1007/978-1-4612-1098-6>, [retrieved 10 Jun. 2024].
- [27] Boyd, S. P., and Vandenberghe, L., *Convex Optimization*, Cambridge University Press, 2004. <https://stanford.edu/~boyd/cvxbook> [retrieved 2 Mar. 2024].
- [28] Pólya, G., “More Isoperimetric Inequalities Proved and Conjectured,” *Comment. Math. Helv.*, Vol. 29, Dec. 1955, pp. 112–119. <https://doi.org/10.1007/BF02564274>.
- [29] Page, J., “Area of a Regular Polygon,” <https://www.mathopenref.com/polygonregulararea.html>, 2024. [retrieved 20 Jun. 2024].
- [30] Zarchan, P., “Boost-Phase Filtering Options: Is Simpler Better?” *Journal of Guidance, Control, and Dynamics*, Vol. 33, No. 6, Nov. 2010, pp. 1724–1731. <https://doi.org/10.2514/1.50190>.
- [31] Lawton, J. A., Jesionowski, R. J., and Zarchan, P., “Comparison of Four Filtering Options for a Radar Tracking Problem,” *Journal of Guidance, Control, and Dynamics*, Vol. 21, No. 4, Aug. 1998, pp. 618–623. <https://doi.org/10.2514/2.4280>.
- [32] Zarchan, P., *Progress in Astronautics and Aeronautics: Fundamentals of Kalman Filtering: a Practical Approach*, Vol. 208, AIAA, 2005. <https://doi.org/10.2514/4.102776>, [retrieved 22 Mar. 2024].